DEUTSCHES ELEKTRONEN-SYNCHROTRON DESY

DESY 67/1
Januar 1967

On the Theory of Photo- and Electroproduction of the N*(1236)

by

F. Gutbrod and D. Simon
Deutsches Elektronen-Synchrotron DESY

2 HAMBURG 52 · NOTKESTIEG 1

On the Theory of Photo- and Electroproduction of the N*(1236)

by

F. Gutbrod and D. Simon*

Deutsches Elektronen-Synchrotron DESY

Abstract

Multipole dispersion relations and the Fredholm determinantal method are applied to the calculation of the transverse part of the γNN^* vertex, using relativistic kinematics. The unphysical cuts of the multipole amplitudes have been approximated by the second-order and fourth-order (box) diagrams containing nucleon and pion exchange. No cut-off is necessary. The results for the magnetic dipole amplitude agree, within the theoretical errors, with those of the static theory, while the electric quadrupole turns out to be resonant too. The behaviour of the transition amplitudes for large momentum transfer is discussed.

*On leave of absence from Institut für Theoretische Physik (I)
Universität Marburg, Germany.

I. INTRODUCTION

The problem of low-energy photoproduction of pions is generally believed to be especially well suited for the application of dispersion theoretic methods. It is therefore astonishing to notice the spread in the predictions made by various authors for experimentally poorly known quantities, as well as the different philosophies invoked to understand one of the few well established facts, namely the magnitude of the resonant magnetic dipole amplitude[1)-8)]. In this paper we intend to increase the number of models and give new values for the electric quadrupole amplitude leading to the final state of the N*(1236), and for the dependence of the two transverse[+)] electroproduction amplitudes on the electron four-momentum transfer. The inclusion of some higher-order perturbation diagrams forms the essential content of this model.

The crucial step in applying multipole dispersion relations (assuming the corresponding scattering phase shift to be known) lies in the determination of the unphysical singularities. It is an empirical fact[4),6)] that by inserting for these singularities the projection of the one-nucleon exchange diagram (NE) Fig. 1a, one gets results in complete disagreement with experiment[†)]. To improve this situation, one may add other one-particle exchange diagrams with higher spin, especially N*-exchange[6),7)] (Fig. 1c). In this case, the electromagnetic properties of the N* are "bootstrapped" almost by themselves, since the inhomogeneous NE-term gives a rather small contribution. The result is therefore highly unstable and the calculation of a form factor quite hopeless[6)].

The present model neglects N* exchange (and all other resonance exchange) completely, and retains only the box diagrams shown in Figs. 2a-b, besides of the nucleon and pion exchanges (Figs. 1a, b).
We motivate this by analogy with Yukawa potential theory: there the lefthand cut (l.h.c.) in a partial-wave amplitude is given by the sum of the l.h.c.'s of all ladder diagrams, and this sum converges for all potential strengths[9)]. Under the additional assumption that the main force in the 3/2, 3/2 πN-scattering channel arises from nucleon exchange, we find it plausible that the diagrams of Figs. 2a and b yield the mostimportant contribution to the l.h.c. among the fourth-order perturbation diagrams.

[+)] We do not consider the longitudinal multipole because of unsolved problems of gauge invariance.

[†)] The reasons for this will be repeated in Section II.

It may seem surprising to assume that the box diagram already provides a good approximation, while the second order is totally misleading. It will be shown in Section II that due to dividing the ampitude by certain threshold factors, the asymptotic behaviour of the second and fourth orders are different with the consequence that the contribution of the second order is very small a priori, while the fourth order may be the leading one.

The hypothesis that the box diagrams, or the box diagrams together with the higher-order ladder diagrams, give us the dominating contribution to the l.h.c. is so attractive because if it works in πN elastic scattering, then the famous CGLN-formula (see Section V Eq. (19)) is at least approximately a consequence of the similarity of the diagrams 2a and c. Whether it works in πN scattering, can be checked by inserting the experimental phase and the calculated lefthand cut into the Omnès-Muskhelishvili solution[10] of a linear integral equation, thereby avoiding the convergence difficulties of the N/D-method. The resulting (nonunitary) amplitude should be close to the (unitary) "input" amplitude described by the phase shift. It is shown in Section IV that this consistency condition is reasonably well fulfilled.

Any dispersion calculation with a fixed lefthand cut will yield the correct boundary value either at threshold or at infinity but not both of them. This well-known drawback makes it desirable to use an alternative method which is based on the knowledge of the perturbation expansion, namely the Fredholm determinantal approach[11]. This is shortly reviewed in Section III, and the results obtained by it are compared with those of the dispersion method in the following sections. Section V contains the results for the photoproduction multipoles, while in Section VI the influence of virtual photon mass on the electroproduction of the N* is investigated.

II. KINEMATICS AND INTEGRAL EQUATION

The four-momenta of the incoming and outgoing particles are indicated in Fig 1a). In the CM-System ($\vec{q} = -\vec{p}_2$) we define

$$E_1 = P_{10}, \quad E_2 = P_{20}$$

$$k = |\vec{k}|, \quad q = |\vec{q}|$$

and $$\lambda^2 = k_\mu k^\mu \leq 0 \qquad \text{for photo- and electroproduction.}$$

The CM-energy W is given by

$$W^2 = S = (P_1+k)_\mu (P_1+k)^\mu$$

and the masses are denoted by

$$M = \text{nucleon mass}, \quad \mu = \text{pion mass}.$$

The definitions of M_{1+} and E_{1+}, the magnetic dipole amplitude and the electric quadrupole amplitude belonging to the isospin 3/2 final state, follow that of Ref.[2]. Simultaneously we consider the πN off-shell partial wave amplitude $f_{1+}(W,\lambda^2)$ with the normalization

$$f_{1+}(W,\mu^2) = \frac{e^{i\delta}\sin\delta}{q}$$

We assume that these amplitudes are analytic functions in the cut W-plane and that their kinematical singularities can be removed by considering

$$\mathcal{M}_{1+}(W,\lambda^2) \equiv M_{1+}(W,\lambda^2)/\rho(W,\lambda^2) \tag{1}$$

$$\mathcal{E}_{1+}(W,\lambda^2) \equiv E_{1+}(W,\lambda^2)/\rho(W,\lambda^2)$$

$$g_{1+}(W,\lambda^2) \equiv f_{1+}(W,\lambda^2)/\rho(W,\lambda^2)$$

with

$$\rho(W,\lambda^2) = W\sqrt{E_1+M}\sqrt{E_2+M}\,kq \tag{2}$$

It has been emphasized repeatedly[12] that this choice of $\rho(W,\lambda^2)$ is not quite correct. $f_{1+}(W,\lambda^2)$ for instance does not vanish at $W = M-\mu$ like q but like $q^{1/2}$, due to the imaginary part of the crossed S-wave. Since the scattering lengths of the πN S-waves are very small, it is reasonable to neglect their contributions at the crossed thresholds and to use $\rho(W,\lambda^2)$ as defined in Eq.(2).

Now we have the integral representation

$$h(W) = h_L(W) + \frac{1}{\pi}\int_{M+\mu}^{\infty} \frac{\mathrm{Im}\, h(W')dW'}{W'-W-i\varepsilon} \tag{3}$$

where h(W) stands for any of the three amplitudes defined in Eq.(1) (the argument λ^2 has been suppressed), and $h_L(W)$ denotes the Cauchy integral over the l.h.c. of the amplitude h(W). As in Ref.[13] we split Im h(W) into its elastic part

$$\Delta h_{el}(W) \equiv h(W)e^{-i\delta^*}\sin\delta^* \tag{4}$$

where δ^* is the complex conjugate of the 3/2, 3/2 scattering phase shift, and into the contribution from three- and more particle intermediate states, $\Delta h_{in}(W)$, which we assume to be a given function of W. Thus we get from(3) and (4) the integral equation

$$h(W) = m(W) + \frac{1}{\pi}\int_{M+\mu}^{\infty} \frac{h(W')e^{-i\delta^*(W')}\sin\delta^*(W')dW'}{W'-W-i\varepsilon} \quad \text{with}$$

$$m(W) = h_L(W) + \frac{1}{\pi}\int_{M+\mu}^{\infty} \frac{\Delta h_{in}(W')dW'}{W'-W-i\varepsilon} \tag{5}$$

The solution is[10]

$$h(W) = m(W)e^{i\delta^*}\cos\delta^* + \frac{1}{\pi\mathfrak{D}(W)} P\int_{M+\mu}^{\infty} \frac{e^{i\delta^*W')}\sin\delta^*(W')\mathfrak{D}(W')m(W')dW'}{W'-W} \tag{6}$$

with

$$\mathfrak{D}(W') = \exp\left\{ -\frac{(W-W_o)}{\pi}\int_{M+\mu}^{\infty} \frac{\delta^*(W')dW'}{(W'-W_o)(W'-W-i\varepsilon)} \right\} \tag{7}$$

The constant W_o is arbritrary.

It is instructive to consider the solution (6) in the case of a real, resonant $\delta(W)$, with m(W) approximated by the projection of an NE-diagram ($m_{NE}(W)$). Due to the kinematical factor $\rho(W,\lambda^2)$ we have

$$m_{NE}(W) \underset{W\to\infty}{=} O(W^{-4})$$

and therefore the numerator of the principal-value integral in Eq. (6) is peaked somewhere above the resonance and vanishes rapidly beyond the peak. The principal-value integral will therefore change sign above the resonance, and so does Im h(W), which is given by

$$\text{Im } h(W) = \sin\delta\left\{m_{NE}(W)\cos\delta + \frac{P}{\pi|\mathfrak{D}(W)|}\int_{M+\mu}^{\infty} \frac{|\text{Im}\mathfrak{D}(W')|m_{NE}(W')dW'}{W'-W}\right.$$

In fact this zero lies very close to the resonance position[4),(6),(13)], and therefore a solution of the form

$$h(W) \approx \text{const}\cdot e^{i\delta}\sin\delta$$

is impossible to obtain under the approximation $m(W) = m_{NE}(W)$. If $m(W) = O(W^{-1})$, the principal-value integral does not necessarily have a zero.

This behaviour of m(W) is also required by the unitary sum rules[14]. Now the lefthand contribution of a box diagram or more generally a ladder diagram has always the desired asymptotic behaviour. This is easily seen, if one calculates the lefthand contribution by subtracting from the total diagram (which behaves like W^{-4} due to Eq.(2)) the Cauchy integral over the righthand cut, which in our cases is always $O(W^{-1})$, since the discontinuity over the physical cut is definite. This property of ladder diagrams is valid for all choices of $\rho(W,\lambda^2)$ as long as $\rho(W,\lambda^2) = O(W^{-1-\varepsilon})$, $\varepsilon > o$, but it is not true for the contributions of unreggeized resonance exchange with spin > 1/2.

Except for accidental cancellations we will have

$$h(W) = O(W^{-1})$$

in contradiction to unitarity for $h(W) = g_{1+}(W,\mu^2)$ and with the assumption of unsubtracted dispersion relations for the other amplitudes. In the next section we describe the determinantal solution which is free from this defect.

III. THE DETERMINANTAL SOLUTION

We first treat the formalism in elastic scattering[11], assuming that for our partial wave all ladder diagrams $f_n(W)$ are given (n = number of vertices).

Writing then

$$N(W) = \sum_{n=2,4}^{\infty} N_n(W)$$

$$D(W) = \sum_{n=0,2}^{\infty} D_n(W) \tag{8}$$

with

$$D_o(W) = 1,$$

$$D_n(W) = -\frac{W-W_o}{\pi} \int_{M+\mu}^{\infty} \frac{N_n(W')\, q'dW'}{(W'-W_o)(W'-W-i\varepsilon)}, \quad n \geq 2 \tag{9}$$

$$N_n(W) = f_n(W) + \sum_{\nu=2}^{n-2} f_\nu(W) D_{n-\nu}(W),$$

it can be shown, provided the sums converge, that N(W) has no righthand cut, and that

$$f(W) = \frac{N(W)}{D(W)}$$

is unitary and has the l.h.c. given by the sum of the ladder diagrams.

Furthermore

$$f(W) \equiv \frac{\sum_{n}^{n_{max}} N_n(W)}{\sum_{n}^{n_{max}} D_n(W)}$$

is unitary, i.e. we have to break off the series for N and D at the same n_{max}. Even if the series converge well, we cannot expect that Re D(W) has the proper zero at the resonance position for $n_{max} = 4$. Under the assumption that D(W) has no zeros on the physical sheet, we can make the identification

$$D(W) = \exp\left\{ -\frac{W-W_o}{\pi} \int_{M+\mu}^{\infty} \frac{\delta(W')dW'}{(W'-W_o)(W'-W-i\varepsilon)} \right\} \qquad (10)$$

where δ is the experimental (real) phase shift. N_n and D_n are calculated as before.

As in the dispersion method we can check consistency since we should have

$$\frac{e^{i\delta}\sin\delta}{q} \cong \frac{\sum_{n=2}^{n_{max}} N_n(W)}{D(W)} . \qquad (11)$$

In electroproduction we need the ladder diagrams $M_n(W)$, which contain an electromagnetic interaction as the first step. Now we have

$$N^{(\gamma)}(W) = \sum_{n=2}^{\infty} N_n^{(\gamma)}(W)$$

$$N_n^{(\gamma)}(W) = M_n(W) + \sum_{\nu=2}^{n-2} M_\nu(W) D_{n-\nu}(W) \qquad (12)$$

with the same $D_n(W)$ as before, and

$$M(W) = \frac{N^{(\gamma)}(W)}{D(W)}$$

with D(W) given by Eq.(10), where M(W) stands for M_{l+} or E_{l+}. Approximating $N^{(\gamma)}(W)$ by the first few terms, M(W) has not the l.h.c. as given by the sum of the corresponding $M_n(W)$. It is therefore important to choose the point of normalization of D(W), W_o, close to the region where the most important lefthand singularities are located, i.e. $W_o = M$ for processes involving one-nucleon exchange.

IV. CONSISTENCY CHECK IN πN-SCATTERING

Two methods of calculating the box graph of Fig. 2c are described in the appendix. The one involves an integration over off-shell partial wave projections of the NE diagram, while in the second method the Mandelstam double spectral functions $\rho_A^{Box}(s,t)$ and $\rho_B^{Box}(s,t)$ are calculated following the Mandelstam iteration scheme[15]. The double spectral functions alone do not determine the diagram, since

$$\int_{(M+\mu)^2}^{\infty} ds' \frac{\rho_A^{Box}(s',t)}{s'-s}$$

diverges. Contrary to the double spectral functions the necessary subtraction function $v_A(t')$ is not fixed by unitarity in the s-channel only. In this respect the perturbation method is not equivalent to the pure S-matrix approach, but both methods become identical after fixing the subtraction function by perturbation theory. Then both methods give numerical results in excellent agreement, thus providing a check for our calculations.

Some remarks about the σ-meson exchange are in order. It has become clear that a satisfactory theory of low-energy πN-scattering needs the exchange of a scalar object in the t-channel with a low mass[16]. If this were a stable meson or a narrow resonance we could include it without difficulty into the box graphs as shown in Fig. 2d. This is impossible, however, if it actually represents the l.h.c. of diagrams like Fig. 3a or 3b. We therefore take it into account only through the diagram 1e, fixing the coupling constants according to[16]. At threshold it gives a contribution of 25 percent to the NE-term; its mass was taken as $\mu_\sigma = 3\mu$. Fig. 4 shows the contributions from diagrams 1d and 1e ("Born terms") in the 3/2, 3/2 channel and the l.h.c. of diagram 2c.

In order to evaluate Eq.(5) we extrapolate the experimental phase shift δ to infinity in the manner shown in Fig. 5, where the experimental points are taken from the analysis of Bareyre at el.[17]. The influence of the unknown high energy limit of Re δ can be estimated in the following way. Let us assume the true phase shift δ' to differ from our δ as given by

$$\text{Re } \delta'(W) = \begin{cases} \text{Re } \delta(W) & \text{for } W \leq W_1 < W_2 \leq W \\ \text{Re } \delta(W) \pm \frac{\pi}{2} & \text{for } W_1 < W < W_2 \end{cases} \qquad (13)$$

The deviation $\pi/2$ was chosen since $0 \leq \lim_{W\to\infty} \mathrm{Re}\delta' < \pi$ seems to be a reasonable limit and our δ has the property $\lim \mathrm{Re}\delta = \pi/2$. Forgetting the inelastic contribution to m(W), we may write for h(W) instead of Eq.(6)

$$h(W) = \frac{1}{\pi \mathcal{D}(W)} \int_L \frac{\mathcal{D}(W')\Delta m(W')dW'}{W'-W} \tag{14}$$

where $\Delta m(W')$ is the discontinuity of m(W) on the l.h.c. denoted by L. By substituting $\mathrm{Re}\delta'$ into $\mathcal{D}(W)$, we obtain

$$h'(W) = \frac{1}{\pi \mathcal{D}'(W)} \int_L \frac{\mathcal{D}'(W')\Delta m(W')dW'}{W'-W}$$

$$= \frac{1}{\pi \mathcal{D}(W)} \left(\frac{W-W_1}{W-W_2}\right)^{\pm 1/2} \int_L \frac{\mathcal{D}(W)\left(\frac{W'-W_2}{W'-W_1}\right)^{\pm 1/2} \Delta m(W')dW'}{W'-W}$$

Taking the worst case $W_2 \to \infty$ and representing $\Delta m(W)$ by a δ-function at W_o, we get for W in the resonance region $W \sim W_R$

$$h'(W) = h(W) \left(\frac{W_R-W_1}{W_o-W_1}\right)^{\pm 1/2}$$

With $W_1 > 14\mu$, $W_r \sim 9\mu$, $W_o = M$ (the static pole alone is known to give already a reasonable approximation to the l.h.c.; a possible small negative residue of a second distant pole makes the error smaller) we get

$$h'(W) = h(W) \cdot (1 \mp 0.17). \tag{15}$$

This indicates the order of magnitude of the expected error in our calculations.

For $\Delta g_{in}(W)$ in Eq.(8) we insert

$$\Delta g_{in}(W) = \left(\mathrm{Im}\, f_{1+}^{(o)} - q\left|f_{1+}^{(o)}\right|^2\right)/\rho(W,\mu^2)$$

with

$$f_{1+}^{(o)} = \frac{e^{2i\delta}-1}{2iq} \tag{16}$$

The results for $f_{1+}(W,\mu^2) = \rho(W,\mu^2)\cdot g_{1+}(W,\mu^2)$ are shown in Fig. 6 and 7.

The Fredholm determinantal solution (F) is seen to agree somewhat better with the "input" amplitude $f_{l+}^{(o)}$ (denoted by I) than the dispersion solution (D), although the σ-meson was not included in the former. To repair the remaining discrepancies one can adjust some parameters. For instance we may include effects of the sixth-order ladder diagram, which can be estimated in the following way: From unitarity we know the imaginary part of the sixth order $g_6(W)$

$$\text{Im } g_6(W) = 2q\rho(W,\mu^2)g_2(W,\mu^2)\text{Re } g_4(W,\mu^2),$$

and we can calculate the high-energy limit of the l.h.c. through the unitary sum rule[14]

$$\lim_{W\to\infty} \int_L^\infty \frac{\Delta g_6(W')dW'}{W'-W} = -\lim_{W\to\infty} \int_{M+\mu}^\infty \frac{\text{Im } g_6(W')dW'}{W'-W} \qquad (17)$$

Representing the l.h.c. of $g_6(W)$ by a pole with the adjustable position W_o' and with a residue determined by (17), one can fit the solution D rather close to I with a value $W_o' \approx -50$ μ. Another way of improving the consistency is to raise the resonance energy by 20 MeV. The relative change of the numerator function N(W) defined in Eq. (8) for $n_{max} = 2$ and $n_{max} = 4$ is given by

$$\frac{N_4(W)}{N_2(W)+N_4(W)} = \begin{cases} -0.06 & \text{at } W = M+\mu \\ -0.12 & \text{at } W = W_r, \end{cases} \qquad (18)$$

thus indicating a good convergence of the series for N(W).

V. PHOTOPRODUCTION MULTIPOLES

We now want to apply the same model to our main subject, the electroproduction of the N*. In the dispersion method we calculate the l.h.c. of the multipoles from Figs. 1a, b and 2a, b. The $\gamma N\bar{N}$-vertex with the nucleon off-shell is set equal to its on-shell value. This additional assumption cannot be checked presently.

Furthermore we must specify the inelastic contributions $\Delta h_{in}(W)$, which we simply take proportional to $\Delta g_{in}(W,\mu^2)$, with the ratios determined by that of the box diagrams at $W\to\infty$. Equally well we could have omitted $\Delta h_{in}(W)$ completely, since the above choice gives a contribution < 5 % at resonance for the dispersion solution.

It is customary to split the multipoles into the contributions arising from NE (Figs. 1a and 2a) which are called $M_{l+,N}$ and $E_{l+,N}$, and into those coming from pion exchange (Figs. 1b, 2b) called $M_{l+,\pi}$ and $E_{l+,\pi}$. We shall discuss these quantities separately, restricting ourselves to $\lambda^2=o$ in this section.

1.) $M_{l+,N}$

The result of the static theory[1] for M_{l+} is

$$M_{l+,N}(W) = \frac{\mu_p-\mu_N}{2f}\frac{k}{q} f_{l+}(W,\mu^2)$$
$$M_{l+,\pi}(W) = o \qquad (19)$$

where μ_p and μ_N are the magnetic moments of the proton and the neutron respectively, and $f^2 = 0.081$. These predictions are known to agree well with experiment[18], and of course one would like to rederive them using relativistic kinematics. Our results for Im $M_{l+,N}(W)$ are plotted in Fig. 8 together with the static prediction (CGLN). The ratio between the determinantal and the dispersion solutions at resonance is approximately the same as in the πN-case, but both curves lie somewhat higher with respect to the desired solution than the ones in Fig. 7. If we include the same corrections due to the sixth-order diagram our predictions will be too high. The deviations are, however, not severe in view of Eq. (15).

2.)$M_{l+,\pi}$

The encouraging result for $M_{l+,N}$ is spoiled by the large imaginary part of $M_{l+,\pi}$, which is resonant too. The dispersion solution yields (see Fig. 9)

$$\text{Im } M_{l+,\pi}(W_r) = 0.17 \text{ Im } M_{l+,N}(W_r)$$

Thus Im $M_{l+}(W_r)$ = Im $(M_{l+,N}(W_r) + M_{l+,\pi}(W_r))$ exceeds the static value by 15 percent without sixth-order corrections. The determinantal solution is not shown in Fig. 9. It differs from the dispersion solution by a factor of 2 at $W = W_r$, and the difference between the cases with $n_{max} = 2$ and $n_{max} = 4$ is now large compared to the πN case:

$$\frac{N_4^\gamma(W_r)}{N_2^\gamma(W_r)+N_4^\gamma(W_r)} = -0.29.$$

This was to be expected since the lefthand singularities of $M_{1+,\pi}$ cannot be approximated by a single pole at W = M, where we have normalised D(W). The convergence of the determinantal method may therefore be much poorer than in the πN-case, and we believe the dispersion method to be the more reliable one in this case.

3.) $E_{1+,\pi}$

The situation is quite similar here to the $M_{1+,\pi}$ case. The dispersion solution for $E_{1+,\pi}$ is shown in Fig. 10, and we have near the maximum of Im $E_{1+,\pi}$

$$R_{E,M} \equiv \frac{\text{Im } E_{1+}(W)}{\text{Im } M_{1+}(W)} \approx \begin{cases} -0.1 & \text{at } W-M = 2\mu \\ -0.08 & \text{at } W = W_r \end{cases}$$

This $R_{E,M}$ is larger than that obtained by Finckler[3], who arrived at $R_{E,M} \approx -0.05$. This value has been shown to give a good description of the experiments with polarized γ's[19]. As to the comparison of the dispersion solution with the determinantal solution the same holds as for $M_{1+,\pi}$.

4.) $E_{1+,N}$

This part of the electric quadrupole cannot reliably be calculated in the present model. The Born term is very small except at high energies, where it is comparable to that of $M_{1+,N}$, and its nearby singularities cancel out. Our estimate of the error Eq.(15) does not hold in this case. In the potential language this situation corresponds to a force of a very short range. If we introduce a slowly varying phenomenological correction at the $\gamma N\bar{N}$ vertex, thus suppressing the short range part, the dispersion solution may be made very small, while $M_{1+,N}$ does not change appreciably.

In summary we can say that our numerical results for M_{1+} and $E_{1+,}$ omitting the pathological $E_{1+,N}$ term, are in qualitative agreement with previous model calculations of a quite different nature, which in turn gave good agreement with experiment. Our model certainly tends to yield predictions that are too high. We think it important to take the higher-order ladder diagrams into account before any attempts are made to improve the situation by adding new particle exchange diagrams. Work in this direction is in progress.

VI. ELECTROPRODUCTION

The calculation of the multipoles M_{1+} and E_{1+} for $\lambda^2 \neq 0$ proceeds in the same way as before. Under the assumption that the electromagnetic off-shell couplings of N and π are again the same as the on-shell ones, $M_{1+,N}$ and $M_{1+,\pi}$ contain the nucleon and pion form factors multiplicatively.
Our numerical evaluation rests on the assumption that

$$G_E^v(\lambda^2) = G_M^v(\lambda^2)/G_M^v(o) \qquad \text{for all } \lambda^2.$$

We think a check of the present model in electroproduction for larger momentum transfer to be more significant than a comparison of small effects in photoproduction. For instance, the determinantal solution for $M_{1+,N}$ in the second-and fourth-order approximations differ by 7 percent at $\lambda^2=0$ and by 23 percent at $\lambda^2 = -100\mu^2$. The λ^2-dependence of our model predictions is therefore more characteristic than the detailed shape of the amplitudes for $\lambda^2=0$. We define form factors $F_{M,N}(\lambda^2)$ by

$$F_{M,N}(\lambda^2) = \left| \frac{\mathcal{M}_{1+,N}(W_r, \lambda^2)}{\mathcal{M}_{1+,N}(W_r, o)} \right| \cdot \frac{G_M^v(o)}{G_M^v(\lambda^2)}$$

and correspondingly $F_{M,\pi}(\lambda^2)$ and $F_{E,\pi}(\lambda^2)$. In Fig.11a some values for $F_{M,N}(\lambda^2)$ are indicated together with an interpolation curve, fitted to the dispersion solutions, of the form

$$F_{M,N}(\lambda^2) = \frac{1}{1-\lambda^2/\Lambda_1^2} \qquad (20)$$

with $\Lambda_1^2 = 140\ \mu^2 = 2{,}72\ (\text{GeV})^2$.

The fact that the determinantal method in fourth order gives lower values for $F_{M,N}(\lambda^2)$ than the dispersion method, can easily be understood. We have, by rearranging terms

$$M_{1+}(W,\lambda^2) = \frac{1}{D(W)} \left\{ M_{1+}^{Born} \left(1+\sum_{\nu=2}^{n_{max}} D_\nu(W)\right) + M_{1+}^{Box} \left(1+\sum_{\nu=2}^{n_{max}-2} D_\nu(W)\right) + \ldots \right\}$$

in obvious notation. Now $\mathrm{Re}(1+D_2(W_r)) = 0.35$, so that for $n_{max} = 4$ M_{1+} is still partly proportional to M_{1+}^{Born} and follows its stronger decrease as a function of λ^2 (see Fig. 11a).

Values of the form factor $F_{M,\pi}(\lambda^2)$ are shown in Fig. 11b together with the fit

$$F_{M,\pi}(\lambda^2) = \frac{1}{1 - \lambda^2/\Lambda_2^2} \quad \text{with } \Lambda_2^2 = 50\ \mu^2 = 0.97\ (\text{GeV})^2 \tag{21}$$

Collecting our results for M_{1+} we find

$$M_{1+}(W,\lambda^2) \approx M_{1+}(W,o)\frac{k}{k_o}\sqrt{\frac{E_1+M}{E_{10}+M}}\left\{\frac{G_M^v(\lambda^2)}{G_M^v(o)}\,\gamma_N F_{M,N}(\lambda^2)+F_\pi(\lambda^2)\,\gamma_\pi F_{M,\pi}(\lambda^2)\right\} \tag{22}$$

with $F_{M,N}$ and $F_{M,\pi}$ approximated by (20) and (21), and

$$\gamma_N \approx 0.85, \quad \gamma_\pi \approx 0.15$$

k_o and E_{10} are k and E_1 evaluated for $\lambda^2 = 0$.
A similar content of "pion terms" in M_{1+} has been found by Menessier[6].

The electric quadrupole (under the neglection of $E_{1+,N}$) is given by

$$E_{1+}(W,\lambda^2) \approx E_{1+}(W,o)\,\frac{k}{k_o}\sqrt{\frac{E_1+M}{E_{10}+M}}\,F_\pi(\lambda^2)F_{E,\pi}(\lambda^2) \tag{23}$$

with

$$F_{E,\pi} \approx \frac{1}{1 - \lambda^2/\Lambda_3^2}\ , \quad \Lambda_3^2 = 80\ \mu^2 = 1.56\ (\text{GeV})^2$$

In the literature one can find the following other predictions:

1) From the behaviour of the Born term alone[2]:

$$M_{1+,N}(W,\lambda^2) \approx M_{1+,N}(W,o)\,\frac{M_{1+,N}^{Born}(W_r,\lambda^2)}{M_{1+,N}^{Born}(W_r,o)}$$

(See Fig. 11a for the difference between this equation and Eq. (22))

2) From a cut-off type theory[5]:

$$M_{1+}(W,\lambda^2) \approx M_{1+}(W,o)\,\frac{k}{k_o}\sqrt{\frac{E_{10}+M}{E_1+M}}\left\{\cdot 94\,\frac{G_M^v(\lambda^2)}{G_M^v(o)}\,C_1(\lambda^2)+0\cdot 06\,F_\pi(\lambda^2)\,C_2(\lambda^2)\right\} \tag{24}$$

with

$$C_1(\lambda^2) = \frac{1}{1 - 0.15\lambda^2}\ , \quad C_2(\lambda^2) = \frac{1.11 - 0.16\lambda^2}{1 - 1.51\lambda^2}, \quad (\lambda^2 \text{in } (\text{GeV})^2)$$

which should be valid for $\lambda^2 < -0.1$ (GeV)^2
Note the different argument of the square root with respect to Eq. (22). The decrease of expression (23) with λ^2 is faster than in Eq. (22).

3) Group theoretical predictions:
From the symmetry group U(6,6)[20] or from collinear groups[21] a connection between the nucleon form factors and the γNN^* transition form factors is obtained. In the notation of Eq.(22) it reads

$$\gamma_N = 1, \ \gamma_\pi = 0 \text{ and } F_{M,N}(\lambda^2) \equiv 1.$$

The deviations from (22) are large for $\lambda^2 < -2$ (GeV)^2.

VII. CONCLUSIONS

It is evident that our attempts to go beyond the static theory of photo- and electroproduction are yet in a preliminary stage. The convergence of the ladder series expansion for either the lefthand cut or for the N^γ-function has been shown neither mathematically nor practically. We only can state that the inclusion of the fourth-order box diagrams drastically improves (as compared to one-particle exchange) the dispersion theoretic prediction towards the experimentally accepted values. In the determinantal method the "convergence" is good in those cases where the subtraction point of the D-function coincides with the location of the dominant nearby singularities, and bad in the other cases.
No attempt has been made to include crossing. The nearby singularities of Diagram 1c are known to be small[1], and the distant ones cannot be calculated. The usual method to derive the multipole dispersion relations from fixed-t dispersion relations seems to avoid this difficulty[4], [6], [7], but this comes from using the multipole expansion of the invariant amplitudes outside the region of convergence. Since no predictions even of the low-energy amplitudes can be made[6] without a definite assumption on the distant singularities it seems better to omit N^*-exchange for the present. These reasons also make the predictions of the form factors too uncertain for determining the neutron form factor from a measurement of the process $\gamma N \to N^*$[22]. The same holds for all quantities connected with the pion form factor.

Appendix

Here we will shortly describe the calculation of the box diagrams. In πN-scattering two different methods have been applied. The first one is based on off-shell partial-wave amplitudes, while the second one uses the Mandelstam iteration procedure. In the case of electroproduction, however, the latter one is too complicated and only the first method was used.

1.) Off-shell method in πN-scattering

For a diagram analogous to Fig. 2c with spin zero particles of equal mass μ we have

$$f^{Box}(W,t) \sim \frac{1}{q^2}\int_0^\infty d\sigma \int_{-\infty}^{\infty} \frac{d\tau}{(b_2^2-\mu^2+i\varepsilon)(b_4^2-\mu^2+i\varepsilon)} \int \frac{d\Omega}{(Z_1-x_1)(Z_1-x_2)}$$

where

$$Z_1(E_2,q) = \frac{(E_2-\tau)^2-E^2-\sigma^2}{2q\sigma}, \quad x_1 = \cos(\vec{p}_1,\vec{b}_2), \quad x = \cos(\vec{p}_2,\vec{b}_2)$$

with

$$t = (p_1-p_2)^2$$

$$q = |\vec{p}_1| = |\vec{p}_2|$$

$$b_{20} = \tau, \quad |\vec{b}_2| = \sigma .$$

Partial wave projection leads to

$$f_1^{Box}(W) \sim \frac{1}{q^2}\int_0^\infty d\sigma \int_{-\infty}^{+\infty} \frac{d\tau}{(b_2^2-\mu^2+i\varepsilon)(b_4^2-\mu^2+i\varepsilon)} \left[Q_1(Z_1)\right]^2$$

The $Q_1(z)$ are Legendre functions of the second kind. Two of the four poles coming from the propagators $\frac{1}{b_2^2-\mu^2}$ and $\frac{1}{b_4^2-\mu^2}$ may pinch the τ-integration contour. We perform a Wick rotation $\tau = u + i\,v$, $-\infty < v < +\infty$ but we have to treat the contour around the two poles carefully. By the Wick rotation the numerical integration along the remaining poles and the logarithmic cuts of the $Q_1(z)$ is avoided. The

point u will be specified by convenience considerations below. In the actual πN case (spin, unequal masses) we use for the intermediate nucleon propagator the following decomposition

$$\not{b}_4+M = \alpha_1(\not{r}_1+M) + \alpha_2(\not{r}_2+M)$$

with

$$r_1^2 = r_2^2 = M^2$$

and

$$\vec{r}_1 = \vec{r}_2 = \vec{b}_4, \quad r_{10} = - r_{20}.$$

This requires

$$\alpha_1 + \alpha_2 = 1$$

$$\alpha_1 = \frac{1}{2} \left(1 + \frac{b_{40}}{\varepsilon}\right)$$

$$\varepsilon = r_{10} = \sqrt{\vec{b}_4^2 + M^2}$$

Now the propagator is the sum of two projection operators, and we have

$$g_{1+}^{\text{Box}}(W,\lambda^2) = \frac{2}{i\pi^2\,\rho(W,\lambda^2)W}\left(\frac{g^2}{4\pi}\right)^2 \int \frac{d\sigma d\tau\ \sigma^2}{(b_2^2-\mu^2+i\varepsilon)(b_4^2-\mu^2+i\varepsilon)} \cdot \tag{A1}$$

$$\cdot\left(\alpha_1 N(E_2,q)N(E_1,k) + \alpha_2 N'(E_2,q)N'(E_1,k)\right)$$

where

$$N(E_2,q) = N_+(E_2,q) + N_-(E_2,q)$$

$$N_{(\pm)}(E_2,q) = \frac{\sqrt{(E_{2(\pm)}M)(\varepsilon_{(\pm)}M)}}{2q\sigma}\,(W'_{(\mp)}M)Q_{1(2)}(Z_1(E_2,q)) \tag{A2}$$

$$Z_1(E_1,k) = Z_2$$

and

$$W' = \varepsilon + \tau.$$

The replacement of ε by $-\varepsilon$ leads from N to N'.

The τ-integration runs from $\tau=u-i\infty$ to $\tau=u+i\infty$, encircling the poles at

$$\tau_1 = \sqrt{\sigma^2 + \mu^2}$$

and $$\tau_2 = W - \sqrt{\sigma^2 + M^2}$$

clockwise and anticlockwise respectively, as long as $\tau_1 \leq u$ or $\tau_2 \geq u$. For the rotation point u we take the center of the gap on the real τ-axis, which lies between the logarithmic singularities of the $Q_1(z_1)$ of Eq. (A2):

$$u = \frac{1}{2}\left[\left(\sqrt{(\sigma-q)^2+M^2}+E_2\right)-\left(\sqrt{(\sigma-k)^2+M^2}-E_1\right)\right] . \qquad (A3).$$

The pinching singularity $\tau_1 = \tau_2$ is removed by subtracting from Eq. (A1) the righthand cut given by

$$g_{1+}^{\text{Box},R}(W,\lambda^2) = \left(\frac{g^2}{4\pi}\right)^2 \frac{1}{\pi} \int_{M+\mu}^{\infty} \frac{dW'}{W'-W} \frac{q'}{W^2\rho(W',\lambda^2)} N(E_2',q')N(E_1',k')$$

where E_1' etc. are functions of W', and for the argument σ of N in Eq. (A2) q' is to be inserted. The l.h.c. of the box diagram is just given by this difference.

2. Mandelstam representation

The Mandelstam representation[15] gives

$$g_{1+}^{\text{Box}}(W,\mu^2) = \frac{W^2-M^2}{\pi} \int\int \frac{dW'dt'W'}{(W'^2-W^2)(W'^2-M^2)} \left[R_1(t')-R_2(t')\right] \rho_A^{\text{Box}}(W',t') +$$

$$+ \frac{1}{\pi} \int\int \frac{dW'dt'W'}{W'^2-W^2} \left[(W-M)R_1(t')+(W+M)R_2(t')\right] \rho_B^{\text{Box}}(W',t') +$$

$$+ \int dt' \left[R_1(t')-R_2(t')\right] v_A(M^2,t')$$

where

$$R_{1(2)}(t') = \frac{1}{\rho(W,\mu^2)} \cdot \frac{Q_{1(2)}(Z_1)}{W(E_{2(\mp)}M)}$$

The indices A and B refer to the usual invariant amplitudes A(s,t) and B(s,t). The double spectral functions $\rho^{Box}_{A,B}(s,t)$ are determined[+)] by the Mandelstam iteration procedure[15] from the NE pole in B(s,t), whereas the subtraction function $v_A(M^2,t')$ is calculated by application of the Cutkosky rule[23] to the πN box graph. The relative difference between both methods in our numerical calculation is about 0.003 at $W = M+\mu$.

3.) Electroproduction

The off-shell method gives for the diagram of Fig. 3a)

$$\mathcal{M}^{Box}_{1+,N}(W,\lambda^2) = \frac{eg^3}{(4\pi)^2} \frac{1}{2i\pi^2 W\rho(W,\lambda^2)} \int \frac{d\sigma d\tau}{(b_2^2-\mu^2+i\epsilon)(b_4^2-\mu^2+i\epsilon)} \frac{\sigma}{2k} \cdot$$

$$\cdot \left[\alpha_1 N(E_2,q)\ M_N + \alpha_2\ N'(E_2,q)\ M'_N\right]$$

The function $N(E_2,q)$ is given in Eq. (A2). The same formula holds for $\mathcal{M}^{Box}_{1+,\pi}(W,\lambda^2)$, $\mathcal{E}^{Box}_{1+,N}(W,\lambda^2)$ and $\mathcal{E}^{Box}_{1+,\pi}(W,\lambda^2)$, with M_N and M'_N replaced by M_π, E_N etc. These quantities, which are proportional to the off-shell magnetic dipole (electric quadrupole) projections of nucleon and pion exchange, are given by

$$M_N = n_1(\tau,\sigma) + n_2(\tau,\sigma)$$

$$M_\pi = -n_4(\tau,\sigma)\ F_\pi(\lambda^2)$$

$$E_N = n_1(\tau,\sigma) - n_2(\tau,\sigma) + n_3(\sigma)\left(Q_1(Z_2)-Q_3(Z_2)\right)\cdot\left[F_1^{\nu}(\lambda^2)-(W-M)F_2^{\nu}(\lambda^2)\right]$$

$$E_\pi = n_4(\tau,\sigma) - n_3(\sigma)\left(Q_1(Z_3)-Q_3(Z_3)\right)\ F_\pi(\lambda^2)$$

where

$$n_1(\tau,\sigma) = 2MG_M^{\nu}(\lambda^2)N(E_1,k) -$$

$$- (W'-W)\left[(\varepsilon-M-\tau)\sqrt{(\varepsilon+M)(E_1+M)}\,Q_1(Z_2) - (\varepsilon+M-\tau)\sqrt{(E_1-M)(\varepsilon-M)}\ Q_2(Z_2)\right]F_2^{\nu}(\lambda^2)$$

$$n_2(\tau,\sigma) = \frac{2}{3}(\varepsilon+M)\sqrt{(E_1-M)(\varepsilon-M)}\ \left(Q_0(Z_2)-Q_2(Z_2)\right)\left[(W+M)F_2^{\nu}(\lambda^2)+F_1^{\nu}(\lambda^2)\right]$$

[+)] Some misprints are contained in Ref.[15], Eq. (3.18a) and (3.18b).

$$n_3(\sigma) = \frac{4}{5}(\varepsilon - M)\sqrt{(E_1+M)(\varepsilon+M)}$$

$$n_4(\tau,\sigma) = \frac{2}{3}(\varepsilon+M)\sqrt{(\varepsilon-M)(E_1-M)}\left[Q_0(Z_3)-Q_2(Z_3)\right]$$

and

$$Z_3 = \frac{\mu^2-M^2+E_1^{\,2}+\sigma^2-(W-E_1-\tau)^2}{2\sigma k}\,.$$

For M_π and E_π we use

$$u = \frac{1}{2}\left[\left(\sqrt{(\sigma-k)^2+\mu^2}+W-E_1\right)-\left(\sqrt{(\sigma-k)^2+M^2}-E_2\right)\right].$$

Our coupling constants and form factors are defined and normalized in the following way:

$F_{1(2)}^{\nu}(\lambda^2)$ = isovector nucleon form factor

$F_\pi(\lambda^2)$ = pion form factor

$$G_M^{\nu}(\lambda^2) = \frac{F_1^{\nu}(\lambda^2)}{2M} + F_2^{\nu}(\lambda^2)$$

$$F_1^{\nu}(0) = 1$$

$$F_2^{\nu}(0) = \frac{\mu'_p-\mu'_N}{2M}$$

$$\mu'_p = 1.78$$

$$\mu'_N = -1.91$$

$$\frac{e^2}{4\pi} = \frac{1}{137}$$

$$\frac{g^2}{4\pi} = 14.5$$

ACKNOWLEDGEMENTS

One of the authors (D.S.) would like to thank Professor H. Joos for the kind hospitality extended to him at DESY. We are grateful for illuminating discussions with Mr. J. Honerkamp on the Fredholm determinantal method.

The numerical calculations have been performed by the IBM 7044 of DESY.

Figure Captions:

1.) One-particle exchange diagrams for pion electroproduction (a - c) and πN-scattering (d,e).

2.) Box diagrams for pion electroproduction (a,b) and πN-scattering (c,d).

3.) Inelastic box diagrams for πN-scattering.

4.) Contributions to $g(w,\mu^2)$ from the lefthand cut of the box diagram ("Box") Fig. 2c and from the sum of the box diagram and the Born terms Fig. 1d,e ("Born + Box").

5.) Scattering phase shift Reδ and absorption parameter $\eta = \exp(-2\mathrm{Im}\delta)$ in the 3/2, 3/2 πN-state. The data points are taken from Ref.[17].

6.) Real part of f_{l+}. Comparison of the two solutions (dispersion and Fredholm) with the "input" Re $f_{l+}^{(o)}$ = Re $e^{i\delta}\sin\delta/q$.

7.) Imaginary part of f_{l+}. Comparison of the two solutions (dispersion and Fredholm) with the "input" Im $f_{l+}^{(o)}$ = Im $e^{i\delta}\sin\delta/q$.

8.) Imaginary part of $M_{l+,N}(W,0)$. Comparison of the two solutions with the CGLN-prediction (1), Eq. (19).

9.) Born term and dispersion solution of $M_{l+,\pi}(W,0)$.

10.) Born term and dispersion solution of $E_{l+,\pi}(W,0)$.

11.) a) Form factor $F_{M,N}(\lambda^2)$ for different models. The drawn curve is the interpolation function of Eq. (20).

b) Form factor $F_{M,\pi}(\lambda^2)$ from the dispersion solution (x). The drawn curve is the interpolation function of Eq. (21).

References:

1.) G.F. Chew, M.L. Goldberger F. Low and Y. Nambu (CGLN) — Phys. Rev. 106, 1345 (1957)

S. Fubini, Y. Nambu and V. Wataghin — Phys. Rev. 111, 329 (1958)

2.) Ph. Dennery — Phys. Rev. 124, 2000 (1961)

3.) P. Finckler — preprint: Purdue University, Lafayette, Indiana (1964)

4.) W. Korth, H. Rollnik, D. Schwela and R. Weizel — preprint: Univ. Bonn (1965)

5.) N. Zagury — Phys. Rev. 145, 1112 (1966) erratum: Phys. Rev. 150, 1406 (1966)

6.) G. Mennessier — Nuovo Cim. 46A, 459 (1966)

7.) A. Donnachie and G. Shaw — preprint: University College London (1965)

8.) P. Stichel — Fortschritte der Physik 13, 73, (1965)

9.) R. Blankenbecler, M. Goldberger, N. Khuri and S. Treiman — Ann. Phys. 10, 62 (1960)

10.) N. Muskhelishvili — Singuläre Integralgleichungen (2. ed.) Akademieverlag Berlin (1965)

R. Omnès — Nuovo Cim. 8, 316 (1958)

11.) J. Schwinger — Phys. Rev. 93, 615 (1954) and ibid. 94, 1362 (1956)

M. Baker — Ann. Phys. 4, 271 (1958)

12.) G. Frye and R.L. Warnock — Phys. Rev. 130, 478 (1963)
M.J. Moravczik — Ann. Phys. 30, 10 (1964)
L.M. Simmons, Jr. — Phys. Rev. 144, 1157 (1966)

13.) F. Gutbrod — Nuovo Cim. 45, 830 (1966)

14.) A. Donnachie and J. Hamilton — Phys. Rev. 138, 678 (1965)
F.A. Berends, A. Dennachie and D. Weaver — preprint: CERN TH. 703 (1966)

15.) S. Mandelstam — Phys. Rev. 112, 1344 (1958)

16.) J. Hamilton, P. Menotti, G. Oades and L. Vick — Phys. Rev. 128, 1861 (1962)

C. Lovelace, R.M. Heinz and A. Donnachie — Phys. Lett. 22, 332 (1966)

17.) Bareyre et al. — Proceedings of the Berkeley Conference (1966)

18.) G. Höhler and W. Schmidt — Ann. Phys. 28, 34 (1964)
19.) W. Schmidt and H. Wunder — Phys. Lett. 20,541 (1966)
20.) A. Salam, R. Delbourgo, and J. Strathdee — Proc. Roy. Soc. (London) A 284, 146 (1965).
R. Oehme — Chicago University preprint EFINS 65-95 (1965)

21.) H.G. Dosch and B. Stech — Z. Physik 189, 455 (1965)

22.) M. Gourdin — Proceedings of the International Symposium on Electron and Photon Interactions at High Energies, Vol. II, Hamburg (1965) p. 304

23.) R.E. Cutkosky — J. Math. Phys. 1, 429 (1960)
W.B. Rolnick — Phys. Rev. Lett. 16, 544 (1966)

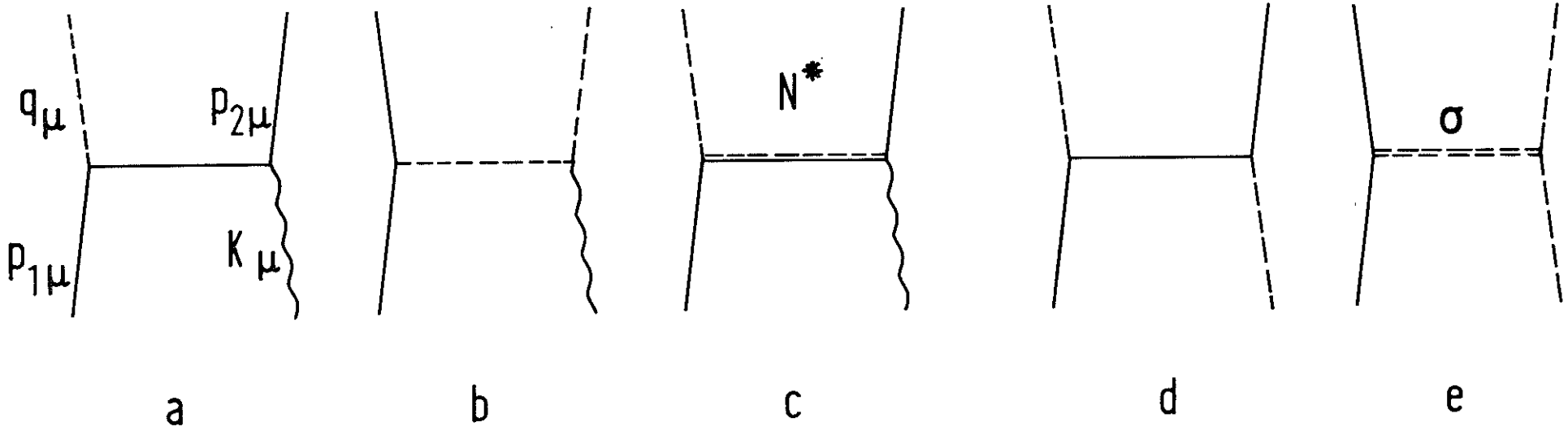

Fig. 1

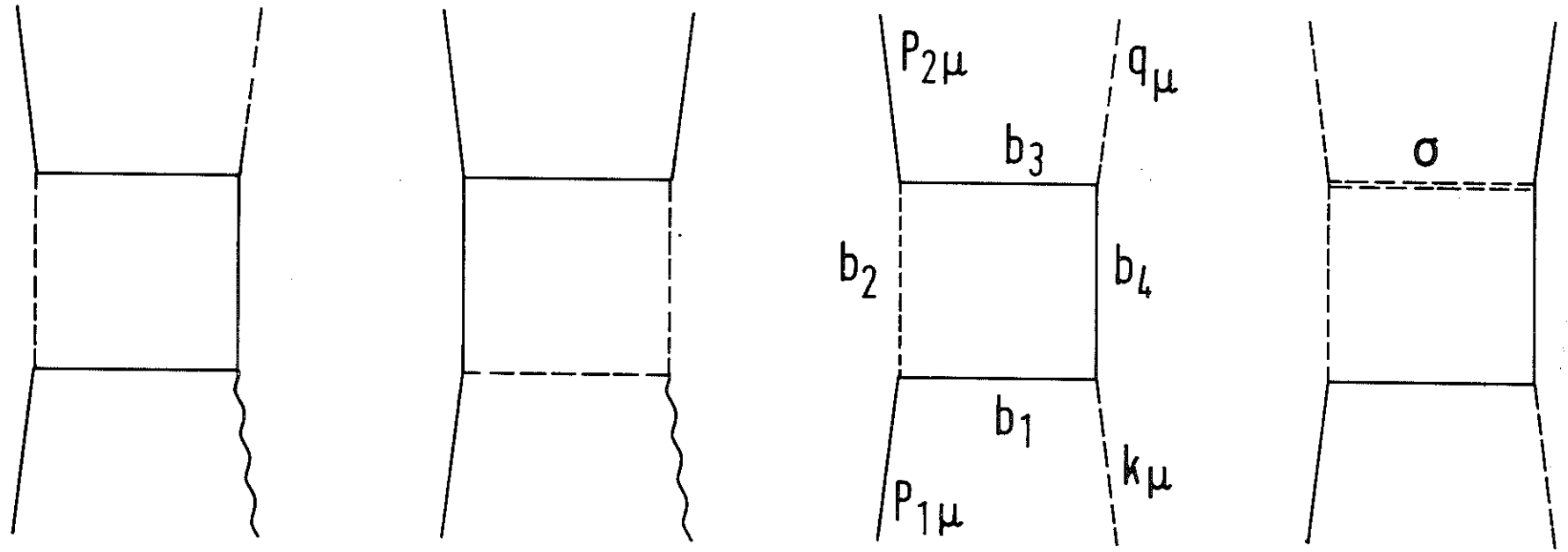

Fig. 2

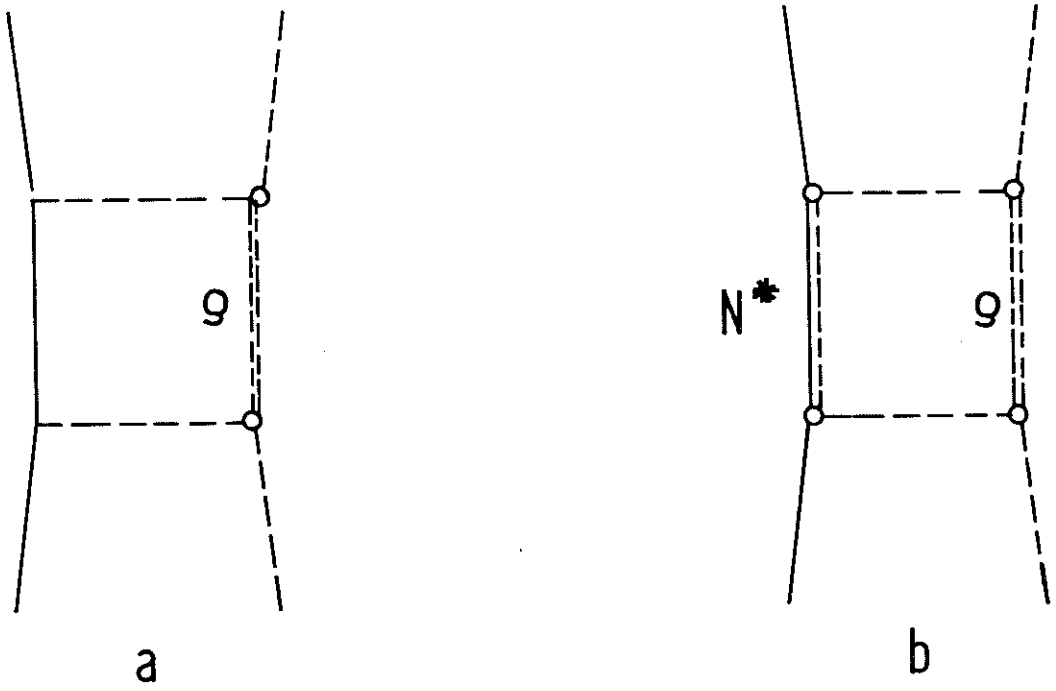

Fig. 3

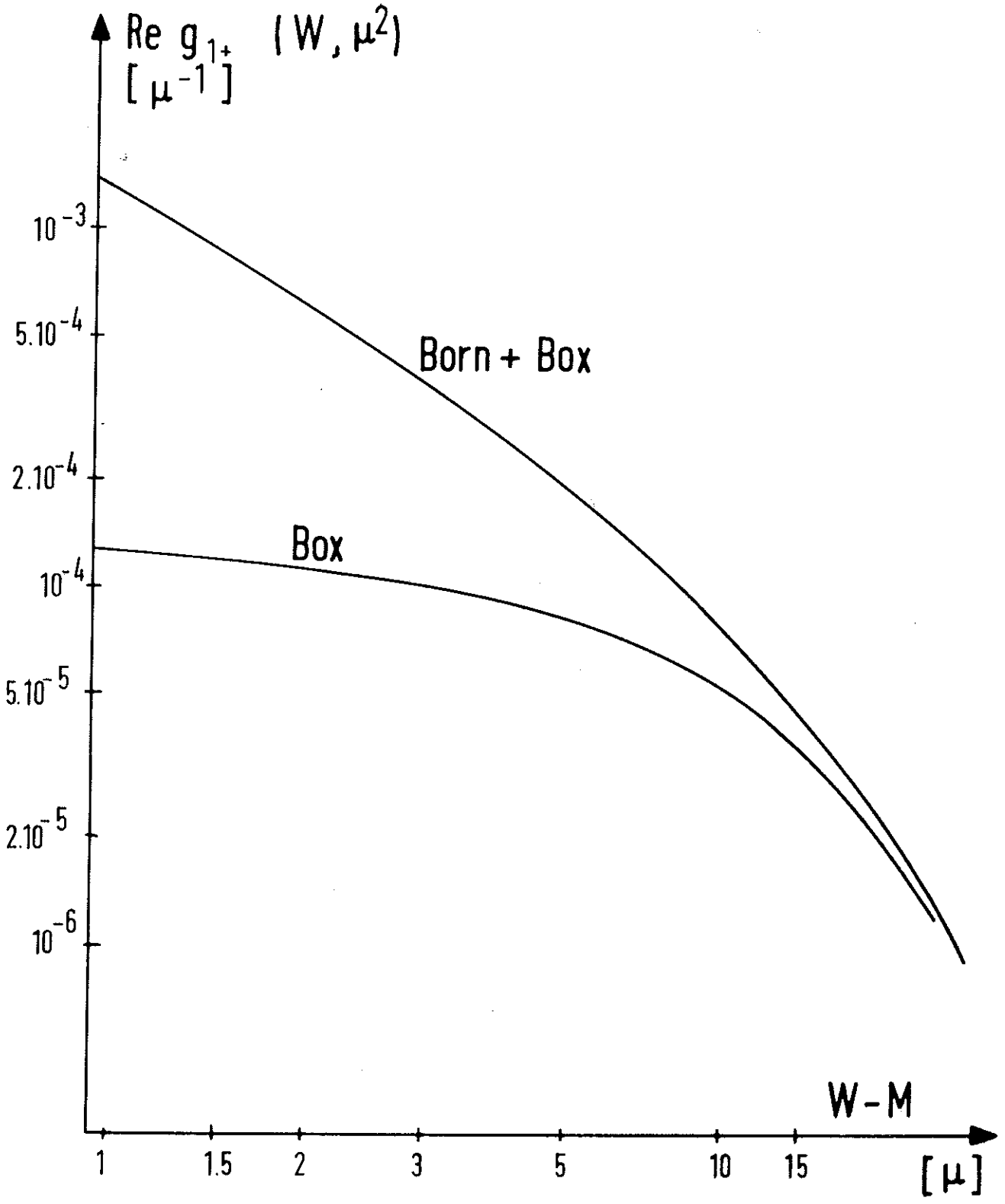
Re g_{1+} (W, μ^2)
$[\mu^{-1}]$
10^{-3}
5.10^{-4}
2.10^{-4}
10^{-4}
5.10^{-5}
2.10^{-5}
10^{-6}
Born + Box
Box
W-M
1
1.5
2
3
5
10
15
$[\mu]$

Fig. 4

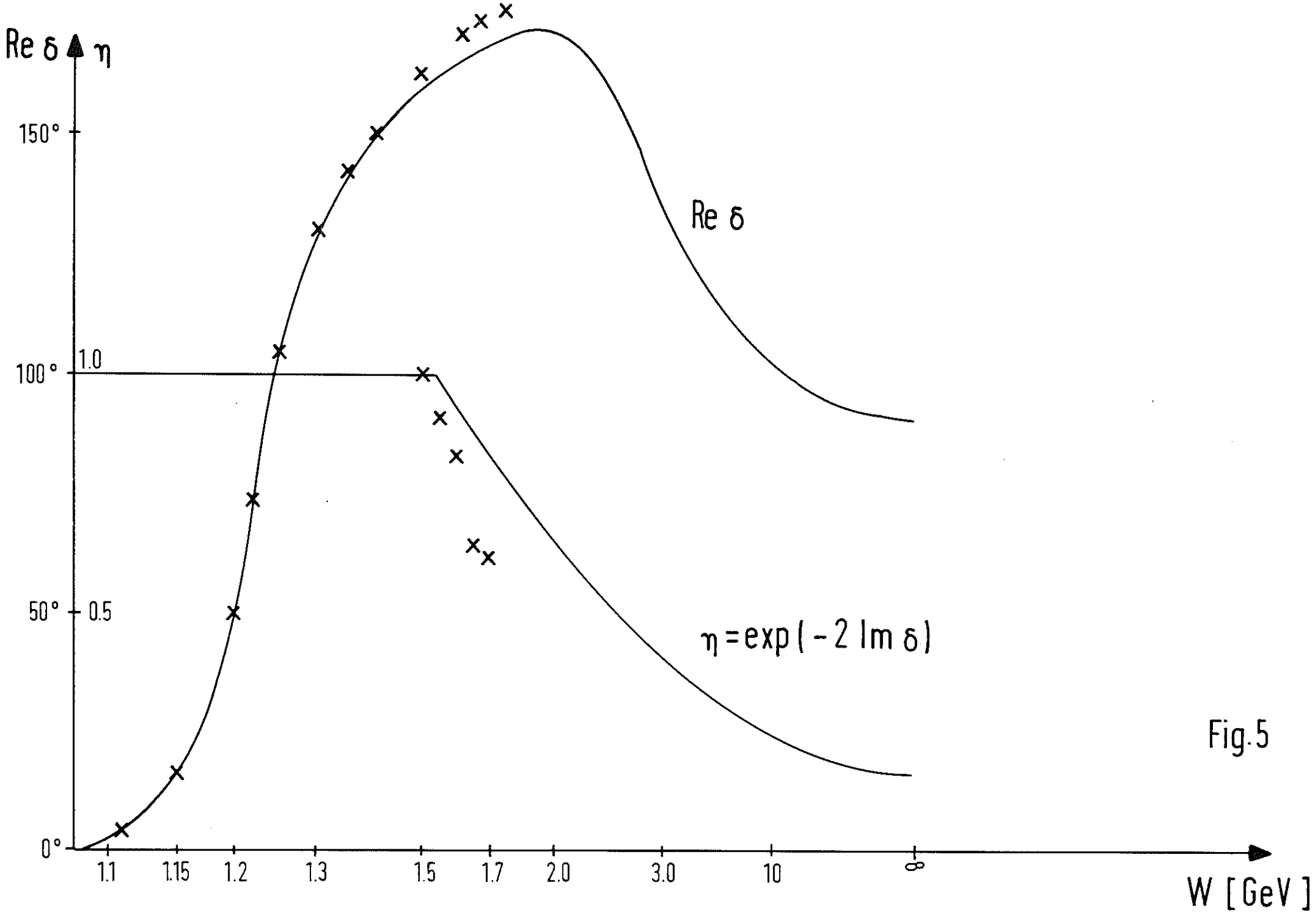
Re δ η
150°
100°
50°
0°
1.0
0.5
Re δ
η = exp (- 2 Im δ)
1.1
1.15
1.2
1.3
1.5
1.7
2.0
3.0
10
∞
W [GeV]

Fig.5

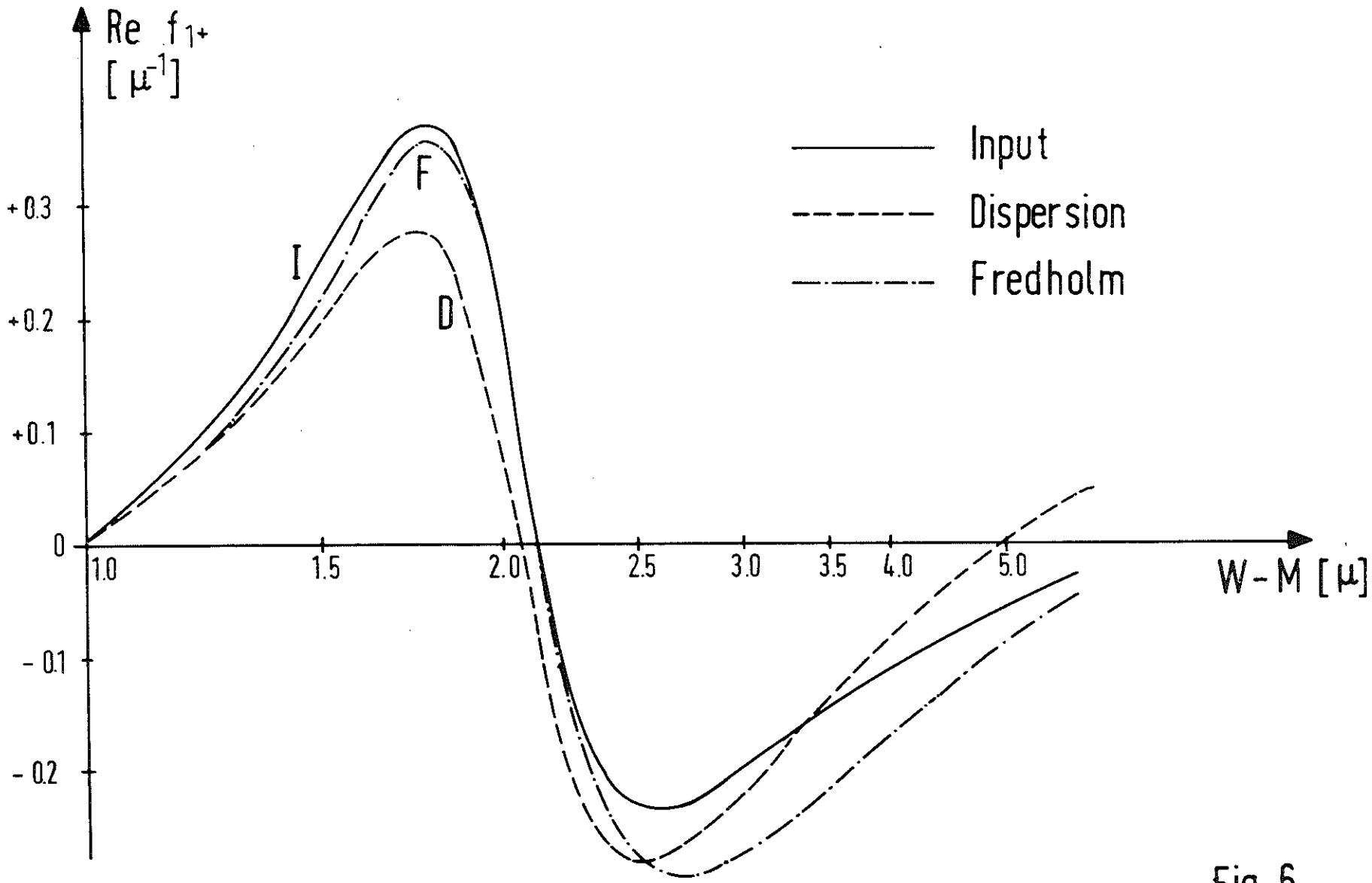
Re f_{1+}
[μ^{-1}]
+0.3
+0.2
+0.1
0
-0.1
-0.2
1.0
1.5
2.0
2.5
3.0
3.5
4.0
5.0
W-M [μ]
I
F
D
Input
Dispersion
Fredholm

Fig. 6

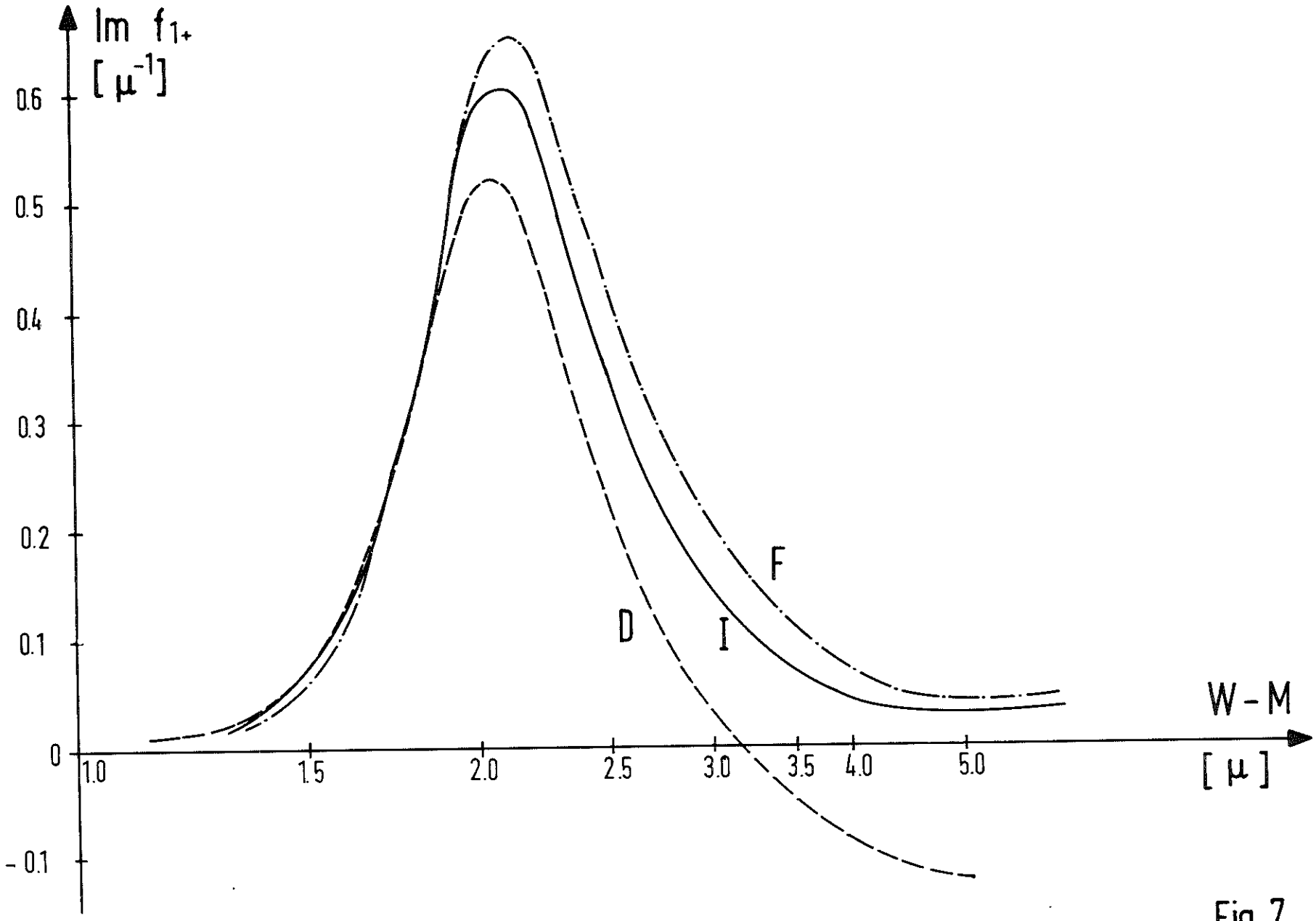

Fig. 7

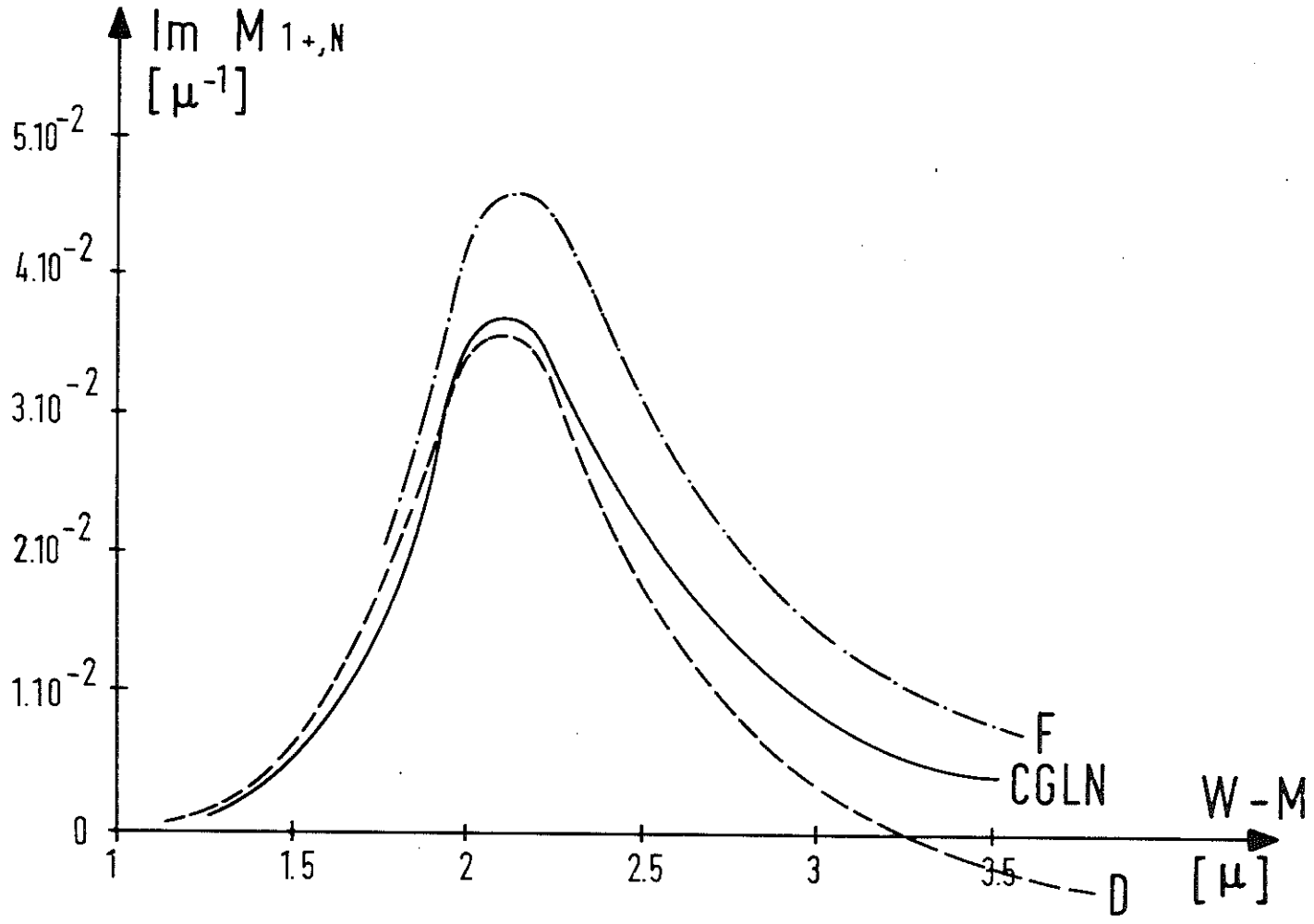

Fig. 8

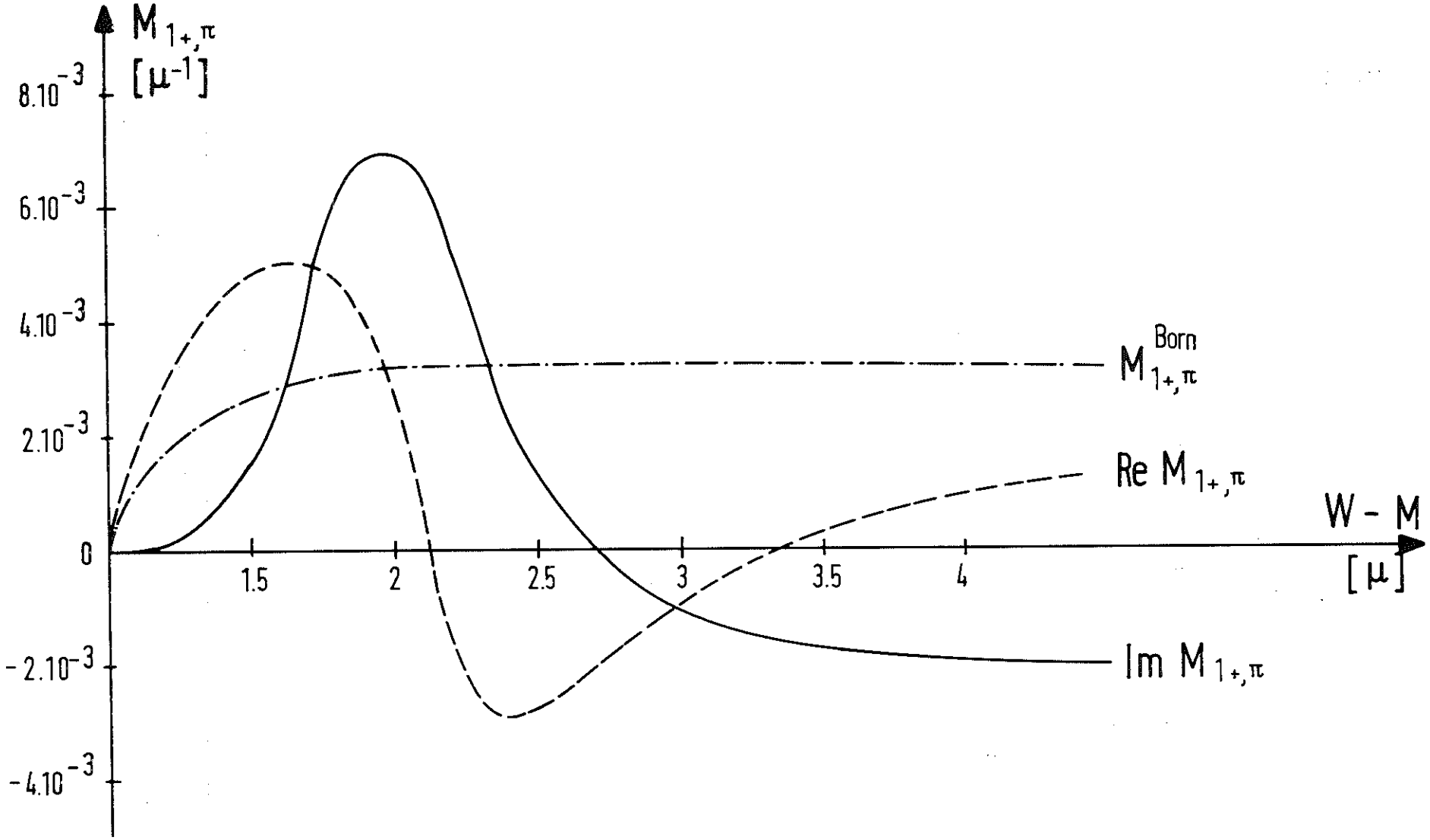
$M_{1+,\pi}$
$[\mu^{-1}]$
8.10^{-3}
6.10^{-3}
4.10^{-3}
2.10^{-3}
0
-2.10^{-3}
-4.10^{-3}
1.5
2
2.5
3
3.5
4
W - M
$[\mu]$
$M^{Born}_{1+,\pi}$
Re $M_{1+,\pi}$
Im $M_{1+,\pi}$

Fig. 9

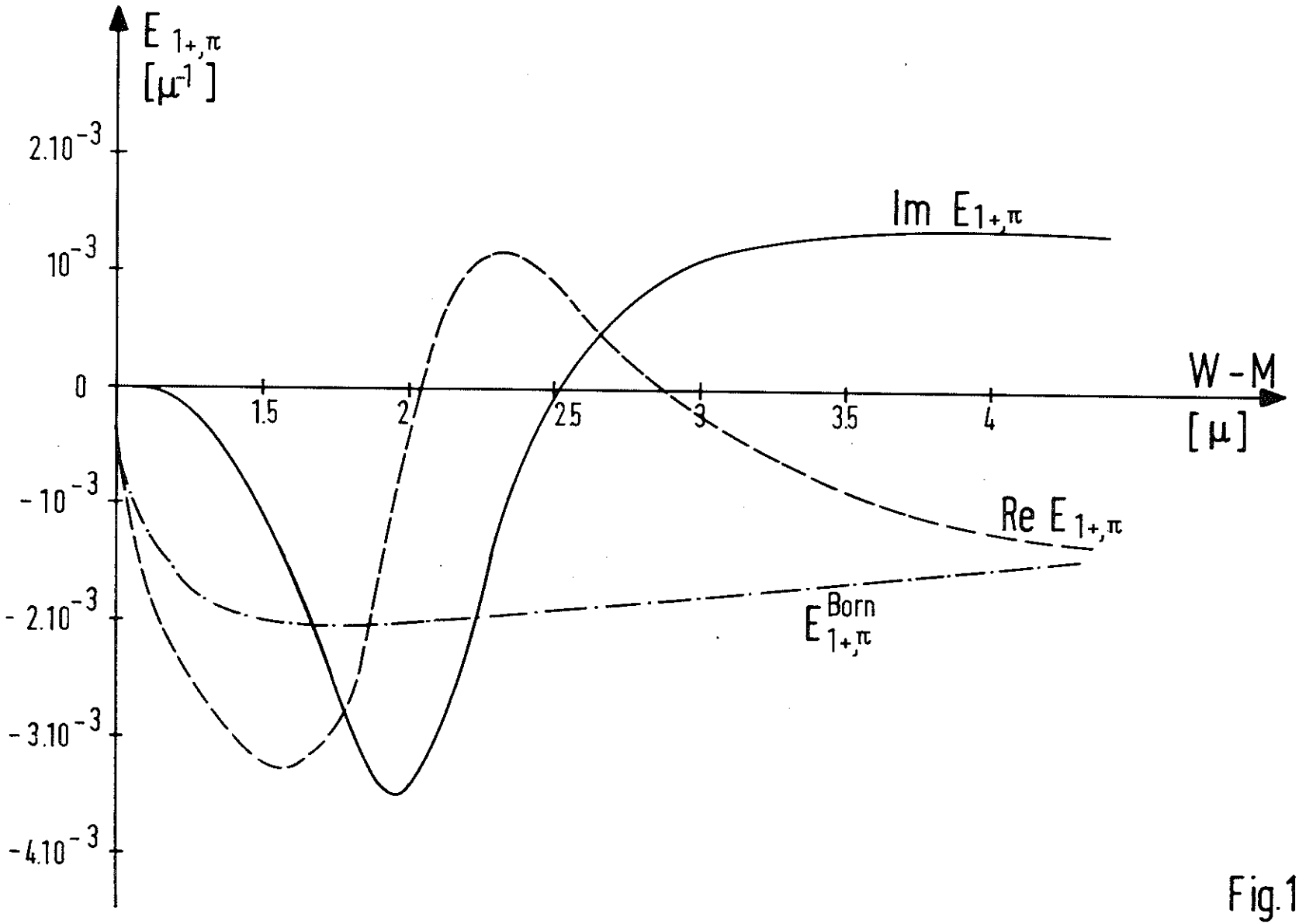
E 1+,π
[μ-1]
2.10-3
10-3
0
-10-3
-2.10-3
-3.10-3
-4.10-3
1.5
2
2.5
3
3.5
4
W-M
[μ]
Im E1+,π
Re E1+,π
EBorn 1+,π

Fig.10

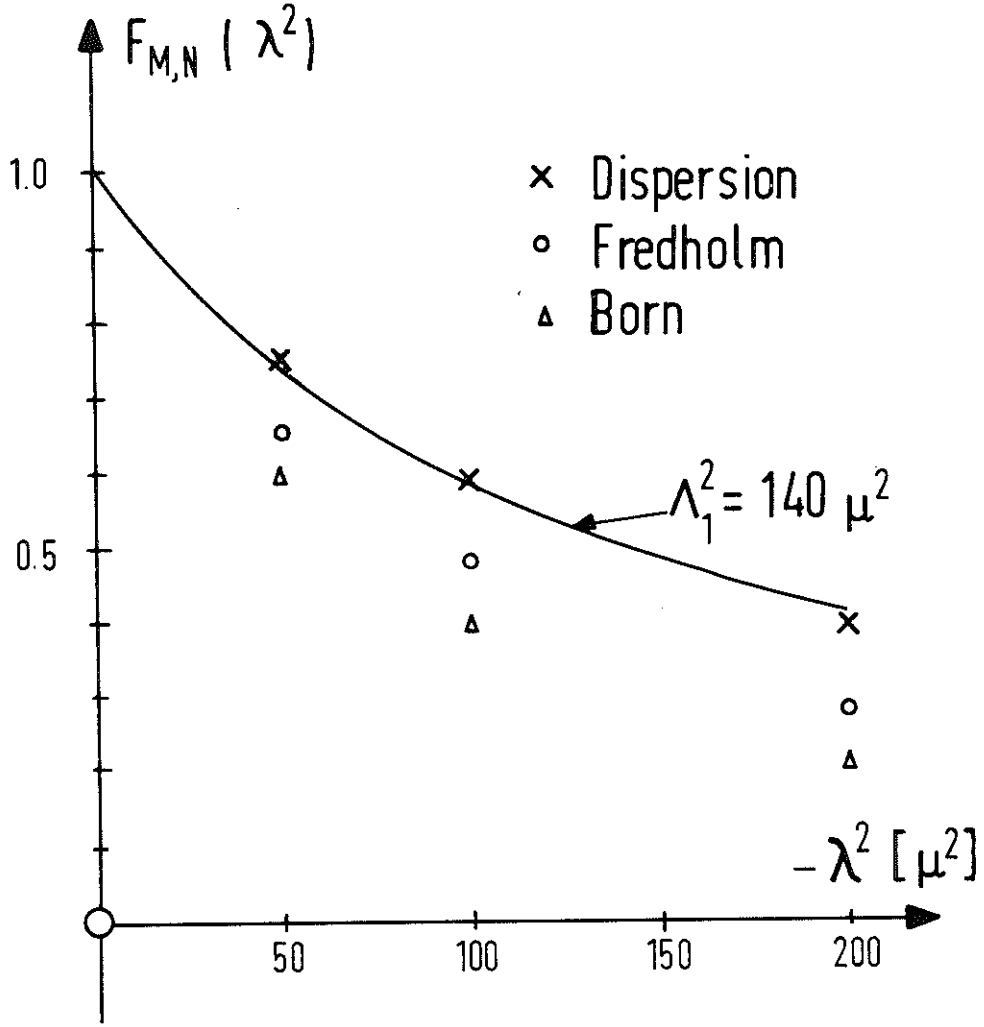
$F_{M,N}(\lambda^2)$
1.0
0.5
× Dispersion
○ Fredholm
△ Born
$\Lambda_1^2 = 140\ \mu^2$
$-\lambda^2\ [\mu^2]$
50
100
150
200

a

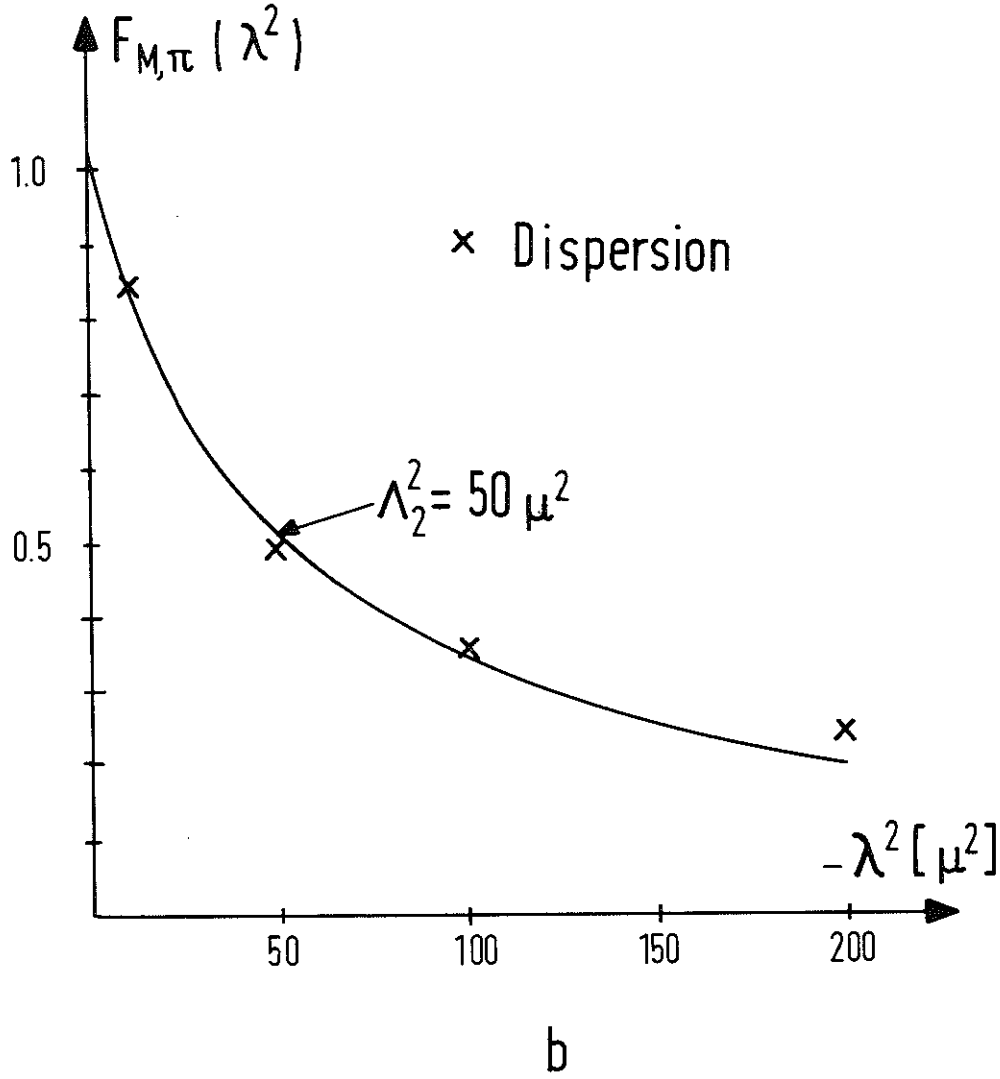
$F_{M,\pi}(\lambda^2)$
1.0
0.5
× Dispersion
$\Lambda_2^2 = 50\ \mu^2$
$-\lambda^2\ [\mu^2]$
50
100
150
200

b

Fig.11

DESY 67/1

E r r a t u m

Fig. 2b should be replaced by the following diagram: